JACS Au
AN OPEN ACCESS JOURNAL OF THE AMERICAN CHEMICAL SOCIETY

pubs.acs.org/jacsau
Article

Electrocatalytic Reduction of Carbon Dioxide in Acidic Electrolyte with Superior Performance of a Metal−Covalent Organic Framework over Metal−Organic Framework

Chang-Pu Wan, Hui Guo, Duan-Hui Si, Shui-Ying Gao, Rong Cao,* and Yuan-Biao Huang

Cite This: *JACS Au* 2024, 4, 2514−2522

ABSTRACT: CO_2 electroreduction (CO_2RR) to generate valuable chemicals in acidic electrolytes can improve the carbon utilization rate in comparison to that under alkaline conditions. However, the thermodynamically more favorable hydrogen evolution reaction under an acidic electrolyte makes the CO_2RR a big challenge. Herein, robust metal phthalocyanine(Pc)-based (M = Ni, Co) conductive metal-covalent organic frameworks (MCOFs) connected by strong metal tetraaza[14]annulene (TAA) linkage, named NiPc−NiTAA and NiPc−CoTAA, are designed and synthesized to apply in the CO_2RR in acidic electrolytes for the first time. The optimal NiPc−NiTAA exhibited an excellent Faradaic efficiency (FE_{CO}) of 95.1% and a CO partial current density of 143.0 mA cm^{-2} at −1.5 V versus the reversible hydrogen electrode in an acidic electrolyte, which is 3.1 times that of the corresponding metal−organic framework NiPc−NiN_4. The comparison tests and theoretical calculations reveal that in-plane full π−d conjugation MCOF with a good conductivity of 3.01×10^{-4} S m^{-1} accelerates migration of the electrons. The NiTAA linkage can tune the electron distribution in the d orbit of metal centers, making the d-band center close to the Fermi level and then activating CO_2. Thus, the active sites of NiPc and NiTAA collaborate to reduce the *COOH formation energy barrier, favoring CO production in an acid electrolyte. It is a helpful route for designing outstanding conductive MCOF materials to enhance CO_2 electrocatalysis under an acidic electrolyte.

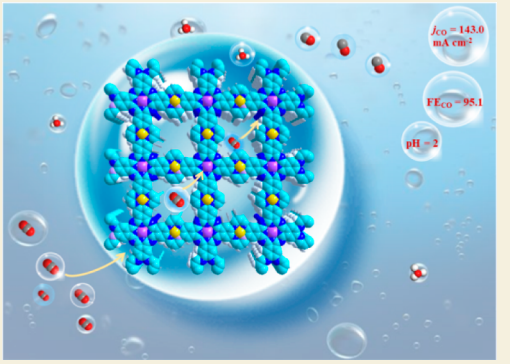

KEYWORDS: *CO_2 electrocatalysis, metal−covalent organic framework, metal−organic framework, phthalocyanine, acidic media*

INTRODUCTION

The electrochemical CO_2 electroreduction reaction can convert CO_2 into valuable chemicals by renewable energy, which is a potential route to realize a carbon-neutral cycle.[1,2] Although CO_2 has strong thermodynamic stability and chemical inertness, the CO_2RR toward the production of CO has achieved great progress recently with high selectivity and industrial-level current density in alkaline or neutral electrolytes.[3−12] However, CO_2 can easily react with local OH^- species in alkaline or neutral electrolytes and cause a serious salting-out effect, which reduces carbon utilization efficiency and greatly impedes the practical viability of alkaline CO_2 electrolysis.[13−18]

In contrast, the CO_2RR in acidic electrolytes can suppress the formation of carbonates to handle the above challenges.[19−32] In acidic electrolytes, hydronium participates in the CO_2RR and hydrogen evolution reaction (HER) rather than H^+, which can inhibit the formation of OH^- and carbonate.[33] Once carbonate is produced locally, it could be converted back into CO_2 molecules when diffused into the bulk acid electrolyte.[34−38] However, the HER at low pH outcompetes the CO_2 electroreduction. Recently, strategies have been designed to boost CO_2RR performance in acidic electrolytes, including electronic structure modulation, surface decoration, nanostructuring, and adding alkali cations. In particular, the single-atom catalysts (SACs) get more attention thanks to maximum atomic efficiency and tunable electronic structure, especially the Ni-based materials. The Ni-SACs exhibit favored kinetics and excellent activity for CO_2 toward CO in acidic electrolytes because of the unique structure and coordination environment.[24,26,30,31] Moreover, Bondue et al. found that HER could be restrained in acidic electrolytes when the rate of CO_2RR was high enough to compensate protons around the catalyst surface.[39] Additionally, Hu et al. reported that adding K^+ ions can suppress HER in an acidic electrolyte.[40] Nevertheless, significant challenges currently remain in achieving favorable levels of current density and

Received: March 17, 2024
Revised: May 16, 2024
Accepted: May 20, 2024
Published: June 21, 2024

https://doi.org/10.1021/jacsau.4c00246
JACS Au 2024, 4, 2514−2522

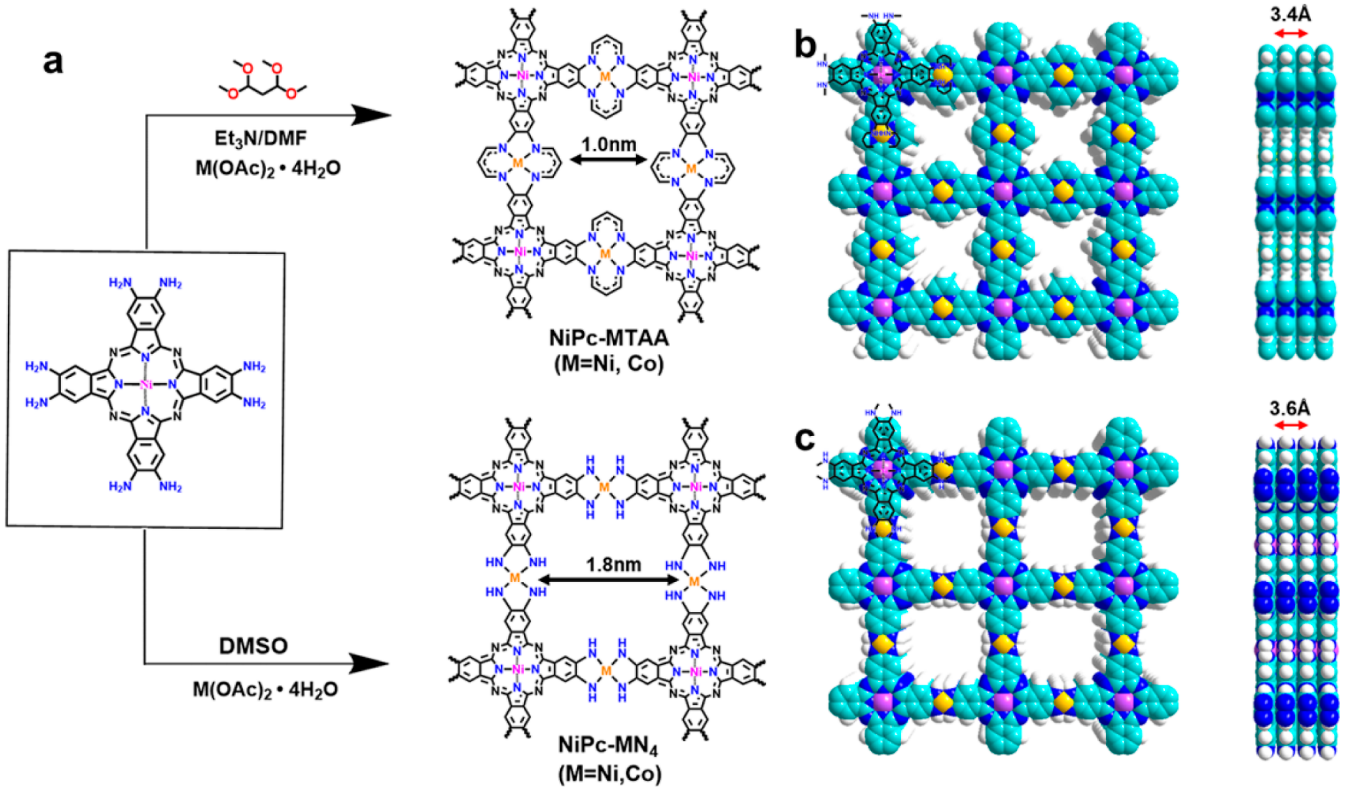

Figure 1. Design and synthesis of the MCOFs NiPc−MTAA (M = Ni, Co) and the MOFs NiPc−NiN_4 and NiPc−CoN_4. (a) Schematic representation for the synthesis of NiPc−MTAA and NiPc−MN_4 under typical solvothermal conditions. (b) Top and side views for 2D crystalline NiPc−MTAA with eclipsed AA stacking patterns. (c) Top and side views of NiPc−MN_4 in AA stacking patterns (C, cyan; N, blue; M, yellow; Ni, purple; H, white).

selectivity. Thus, development of catalysts that can adapt to acidic electrolysis is urgent.

Recently, porous crystalline materials, including metal−organic frameworks (MOFs) and covalent organic frameworks (COFs) linked by periodically arranged functional building blocks, have garnered considerable interest as suitable catalysts for CO_2RR thanks to their high surface areas, high CO_2 adsorption, and tunable active sites.[41−53] Nevertheless, despite MOFs being able to obtain ideal structures and functionalities because of different metal nodes/clusters and organic monomers, their practical implementations are often restricted by the relative weak strength of the coordination bond, particularly in acidic electrolytes for CO_2RR. Meanwhile, although COFs linked by covalent bonds possess more chemical stability in harsh conditions compared with most of MOFs, their poor electron-transfer ability and lack of metal sites usually lead to low current density that cannot meet the requirements of commercial applications.[54−56] Interestingly, metal-covalent organic frameworks combine the advantages of MOFs and COFs to against harsh chemical environments, such as strong acids and bases.[57] Thus, we believe that metal-covalent organic frameworks (MCOFs) can be applied in electrocatalytic CO_2 under acidic electrolytes but not been reported up to now.

Herein, active Ni-phthalocyanine (NiPc) as building block was embedded into two porous conductive MCOFs (NiPc−MTAA, M = Ni, Co, Figure 1) connected by nickel or cobalt tetraaza[14]annulene linkage for the efficient CO_2RR toward the CO_2-to-CO conversion in acidic electrolyte. Due to the high delocalized in-plane d−π conjugation and macrocyclic π conjugation with coordination and covalent bonds, the robust NiPc−MTAA with two types of active sites (NiPc and M-TAA) have better electron-transfer capability and chemical stability than their corresponding MOFs, NiPc−MN_4 (M = Ni, Co, Figure 1) that link with Ni/Co-*o*-phenylenediamine. Thus, the optimal MCOF, NiPc−NiTAA, exhibits an outstanding CO Faradaic efficiency (FE_{CO}) of 98.3% at −1.1 V and an industrial-level CO partial current density (j_{CO}) of 143.0 mA cm^{-2} at −1.5 V in acidic electrolyte, which are greater than that for the corresponding MOF, NiPc−NiN_4 with FE_{CO} = 88.5% and j_{CO} = 46 mA cm^{-2}. Moreover, the MCOF, NiPc−CoTAA, also displays superior FE_{CO} (FE_{CO} = 94.7% at −1.3 V and j_{CO} = 89.0 mA cm^{-2} at −1.5 V) over NiPc−CoN_4 (FE_{CO} = 93.6% at −1.3 V, j_{CO} = 64 mA cm^{-2} at −1.5 V). All these results indicate that the MCOFs, NiPc−MTAA with in-plane π−d conjugation, show better CO_2RR performance in acidic electrolyte compared to the corresponding MOF, NiPc−MN_4. The comparison tests and DFT calculations prove that NiTAA linkage endows the MCOFs with good conductivity due to high d−π orbital overlap between metal sites and TAA, which makes electron transfer continuous along the bonds. Moreover, the d-band center of Ni sites in NiPc−NiTAA is closer to the Fermi level, indicating that the Ni sites have a strong ability to activate CO_2, thereby enhancing the reactivity of Ni sites in acidic electrolytes.

RESULTS AND DISCUSSION

The two MCOFs, NiPc−MTAA (M = Ni, Co), were synthesized using 2,3,9,10,16,17,23,24-octaaminophthalocyaninato nickel(II) (NiPc−$(NH_2)_8$) with tetramethoxypropane (TMP) and metal acetate tetrahydrate under typical

https://doi.org/10.1021/jacsau.4c00246
JACS Au 2024, 4, 2514−2522

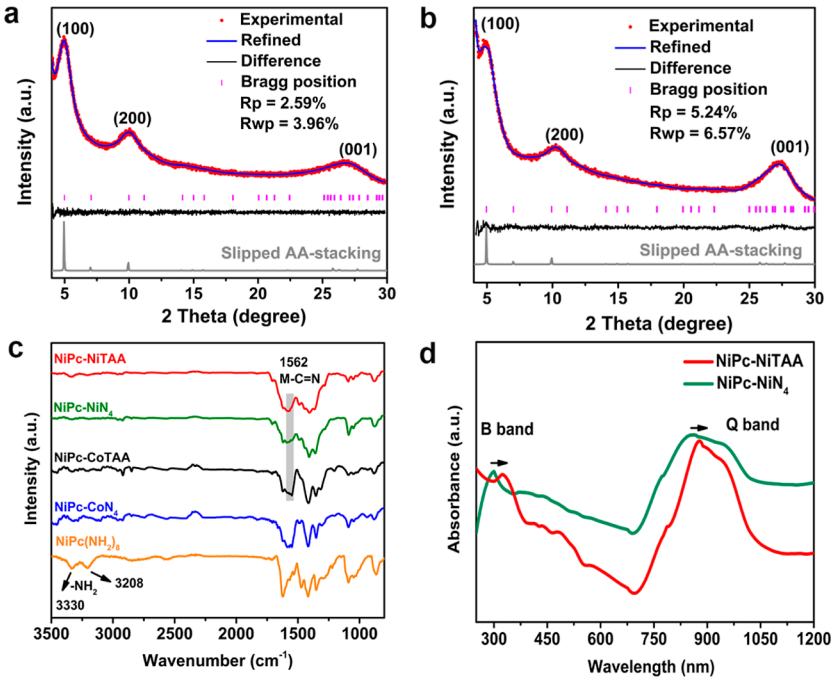

Figure 2. Tested (red), Rietveld-refined (blue), and simulated (gray) PXRD patterns of (a) NiPc−NiTAA and (b) NiPc−NiN_4. (c) FT-IR spectra for NiPc−CoN_4, NiPc−CoTAA, NiPc−NiN_4, NiPc−NiTAA, and the NiPc−$(NH_2)_8$ monomer. (d) UV−vis absorption spectra of NiPc−NiTAA and NiPc−NiN_4.

solvothermal vacuum conditions at 120 °C for 5 days (Figure 1). Additionally, the two corresponding MOFs, NiPc−MN_4 (M = Ni, Co), were also synthesized according to the literature (Figure 1).[58] The formation of these NiPc-based MCOFs (NiPc−NiTAA) and MOFs (NiPc−NiN_4) were confirmed by powder X-ray diffraction (PXRD, Figure 2a,b). The PXRD pattern (Figure 2a) for NiPc−NiTAA was consistent with the simulated slipped AA-stacking model built by Materials Studio 8.0 with the P_4/mmm space group where a = 18.0 Å, b = 18.0 Å, c = 3.48 Å, and $\alpha = \beta = \gamma = 90°$. Moreover, NiPc−CoTAA and NiPc−CoN_4 have the same topology and PXRD patterns as NiPc−NiTAA and NiPc−NiN_4 (Figure S1). The Rietveld refinements for NiPc−NiTAA had validity differences (R_p = 2.59% and R_{wp} = 3.96%), indicating that the slipped AA-stacking model was reliable. In Figure 2a, two obvious diffraction peaks are shown at 4.9 and 10.0°, which were assigned to the (100) and (200) facets, respectively. Additionally, a peak appeared at 28.0°, which could be attributed to the (001) facet. The space-filling structural model of NiPc−MTAA in Figure 1b shows a one-dimensional tetragonal channel with ca. 1.0 nm theoretical pore sizes and a 3.4 Å layer stacking distance (Figure 1b, right side). The experimentally observed PXRD results matched with the simulated pattern, suggesting successful construction of NiPc−MTAA with the metal tetraaza[14]annulene linkage. The MOF NiPc−NiN_4 showed similar PXRD patterns (Figure 2b) as those of NiPc−NiTAA (Figure 2a), which possessed a 1.8 nm pore size and a 3.6 Å interlayer spacing.

The successful syntheses of NiPc−MTAA and NiPc−MN_4 were further validated by Fourier transform infrared (FT-IR) and ultraviolet−visible (UV−vis) spectra. As shown by FT-IR in Figure 2c, the absence of the N−H vibrations located at 3330 and 3208 cm^{-1} in both NiPc−MTAA and NiPc−MN_4 suggested that the amino groups in NiPc−$(NH_2)_8$ were coordinated with the metal ions. Moreover, the spectra of both NiPc−NiTAA and NiPc−CoTAA showed a typical M−C═N peak centered at 1562 cm^{-1}, implying the existence of MTAA.[59] Besides, the UV−vis spectra in Figure 2d showed distinct red shifts for B and Q bands in NiPc−NiTAA compared with NiPc−NiN_4, which suggested that the introduction of the metal-tetraaza[14]annulene linkage endowed MCOF with stronger conjugation.[60] The extended in-plane d−π and macrocyclic π-conjugation across the framework could improve the electron transport capability of NiPc−NiTAA (Figure S2 and Table S1), resulting in high electrical conductivity (3.01×10^{-4} S m^{-1}), which was much higher than for the corresponding MOF NiPc−NiN_4 (2.27×10^{-5} S m^{-1}). The conductivity proved that the MCOFs exhibited better electron transport ability than the corresponding MOFs. Furthermore, electron conductivity of the MCOFs and MOFs was tested by electrochemical impedance spectroscopy (EIS). As per the EIS Nyquist plots shown in Figure S3, NiPc−NiTAA exhibited a smaller semicircle than NiPc−NiN_4. Additionally, NiPc−CoTAA also showed lower charge-transfer resistance (R_{ct}) than NiPc−CoN_4, which could explain the fast electron transfer in MCOFs. Such superior electron conductivity for NiPc−MTAA could facilitate electron transfer to electrodes and CO_2, hence promoting current density for the CO_2RR compared with those of conventional insulating MOFs and COFs. Inductively coupled plasma-optical emission spectrometry proved that NiPc−NiTAA and NiPc−NiN_4 have high densities of active Ni sites with 13.21 and 14.32 wt %, respectively, which would be favorable for the enhancement of current density (Table S2). Elemental analysis demonstrated that carbon, hydrogen, and nitrogen were present in NiPc−MTAA and NiPc−MN_4 (Table S2). Chemical stability of NiPc−MTAA and NiPc−MN_4 was examined by immersing them into 2 M H_2SO_4 solutions. According to the PXRD patterns from Figure S4, NiPc−NiTAA and NiPc−CoTAA still possessed crystallinity under

https://doi.org/10.1021/jacsau.4c00246
JACS Au 2024, 4, 2514−2522

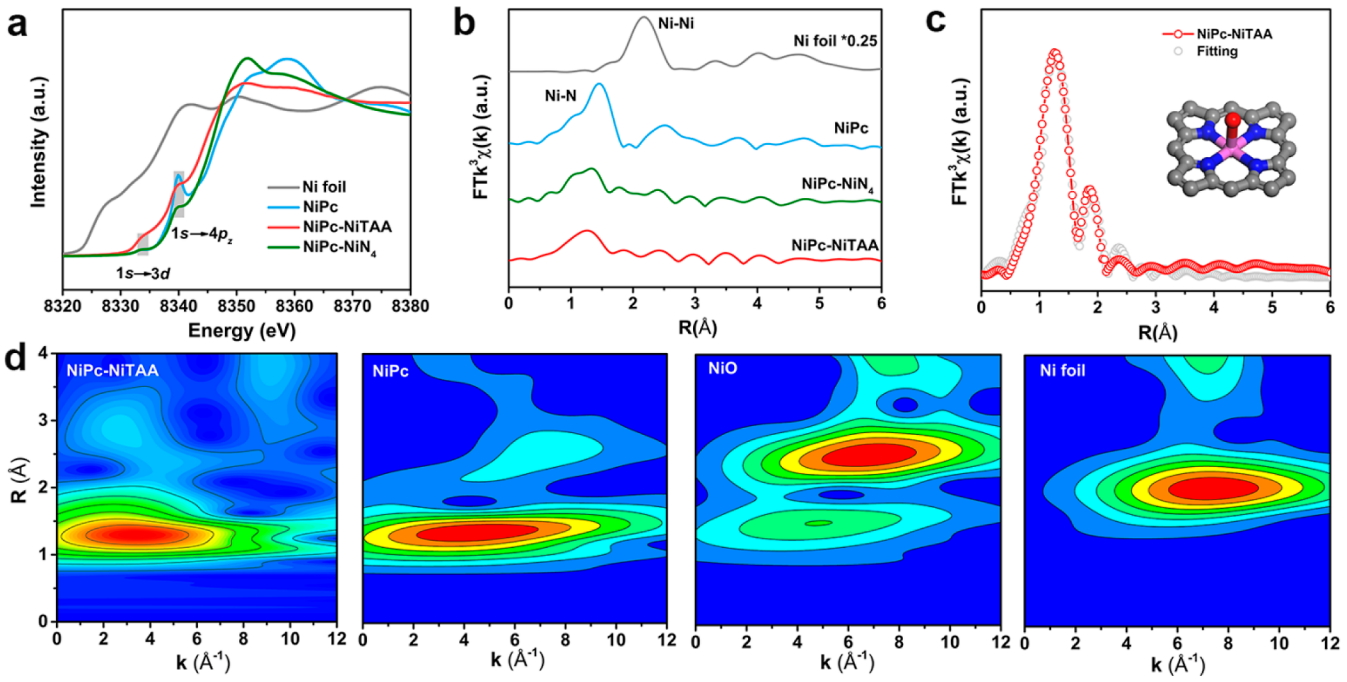

Figure 3. (a) Ni K-edge XANES spectra for Ni-based samples. (b) Ni K-edge of EXAFS spectra for Ni-based samples. (c) EXAFS fitting curve for NiPc−NiTAA [inset diagram for coordination mode: Ni (lilac), O (red)]. (d) WT EXAFS spectra for Ni-based samples.

the strong acidic solution, while the MOF NiPc−MN_4 became amorphous after immersion under the same conditions. These results indicated that the MTAA linkage could enhance the chemical stability of MCOFs. Additionally, thermogravimetric analysis (TGA) indicated that NiPc−NiTAA could be stable up to 400 °C (Figure S5), which was higher than NiPc−NiN_4 (260 °C) and NiPc−CoN_4 (270 °C). Based on the above results, the thermal and chemical stabilities of MCOFs were enhanced by implanting tetraaza[14]annulene into the porous frameworks. Thus, NiPc−NiTAA and NiPc−CoTAA with high chemical and thermal stabilities have great potential to perform electrocatalytic CO_2RR under acidic electrolytes.

Scanning electron microscopy (SEM) images of NiPc−MTAA and NiPc−MN_4 in Figure S6 show irregular stacked layer structures, which were supported by transmission electron microscopy (TEM) in Figure S7a. The MCOFs and their corresponding MOFs had similar morphologies (Figures S6−S8). High-resolution TEM showed no obvious metal nanoparticles (NPs) in NiPc−NiTAA (Figure S7b), which agreed well with the PXRD result. The EDS elemental mapping (Figure S7c) proved that carbon, nitrogen, and nickel elements were uniformly distributed in NiPc−NiTAA. To investigate the CO_2 affinity of the materials, CO_2 adsorption tests were performed at 298 K. In Figure S9, NiPc−NiTAA displayed the highest CO_2 adsorption value of 15.2 $cm^3\ g^{-1}$ over NiPc−NiN_4 (11.1 $cm^3\ g^{-1}$), NiPc−CoTAA (12.1 $cm^3\ g^{-1}$), and NiPc−CoN_4 (6.90 $cm^3\ g^{-1}$). The good CO_2 affinity made NiPc−NiTAA a promising platform for the CO_2RR via enhancing the uptake of CO_2.

To investigate the coordination environments and electronic structure of Ni atoms in NiPc−NiTAA, X-ray absorption spectra were obtained. As shown in Figure 3a, the Ni K-edge XANES spectra in NiPc−NiTAA, NiPc−NiN_4, and NiPc exhibited a pre-edge peak at 8333 eV, which was assigned to the dipole forbidden 1s to 3d transition. Moreover, the shoulder peak located at 8339 eV was associated with the 1s to $4p_z$ electronic transition in NiPc−NiTAA, NiPc−NiN_4, and the NiPc molecule.[58,61] It indicated that a NiN_4 symmetrical structure existed in NiPc−NiTAA and NiPc−NiN_4. Meanwhile, the Ni XANES curves of NiPc−NiTAA and NiPc−NiN_4 was close to that of NiPc, indicating the same bivalent Ni in NiPc−NiTAA, NiPc−NiN_4, and NiPc. The coordination structure of Ni in NiPc−NiTAA was confirmed by EXAFS.

As shown in Figure 3b, the peak at 1.34 Å in NiPc−NiTAA and NiPc−NiN_4 indexed to the characteristic Ni−N. Moreover, the corresponding *R* values were slightly shifted in NiPc−NiTAA and NiPc−NiN_4 in comparison with Ni−N (1.45 Å) in NiPc, attributing to shorter Ni−N bond in the NiTAA node and NiN_4 node. Furthermore, no signal at 2.17 Å from Ni−Ni showed in NiPc−NiTAA and NiPc−NiN_4, suggesting that Ni was not in nanoparticle aggregates. Additionally, based on the EXAFS fitting spectra in Figure 3c and Table S3, the Ni in NiPc−NiTAA was coordinated with four N and one O (Ni−N_4−O). As shown in Figure 3d, the Ni−N/O bonding was observed at 3.5 $Å^{-1}$ and no Ni−Ni at 7.6 $Å^{-1}$ existed in NiPc−NiTAA from wave transform-extended X-ray absorption fine structure (WT-EXAFS), further illustrating the isolated atomic-level dispersion of Ni in the porous framework.

X-ray photoelectron spectroscopy (XPS) was used to illustrate surface compositions and chemical states for NiPc−NiTAA and NiPc−NiN_4. As shown in Figure S10a, the XPS survey spectra of NiPc−NiTAA and NiPc−NiN_4 displayed the peaks of carbon, nitrogen, oxygen, and nickel, which were in accordance with the TEM EDS results. The existence of the O signal came from the coordinated H_2O to the framework. The Ni 2p spectrum of NiPc−NiTAA displayed two main peaks centered at 855.3 eV (Ni $2p_{3/2}$) and 872.6 eV (Ni $2p_{1/2}$), indicating the nickel divalent. Similarly, the Ni 2p spectrum curve for NiPc−NiN_4 showed two peaks at 855.2 and 872.7 eV belonging to Ni $2p_{3/2}$ and Ni $2p_{1/2}$, suggesting a valence of +2 instead of other valence states in the framework (Figure S10b). The N 1s XPS spectrum of NiPc−NiTAA showed that C−

https://doi.org/10.1021/jacsau.4c00246
JACS Au 2024, 4, 2514−2522

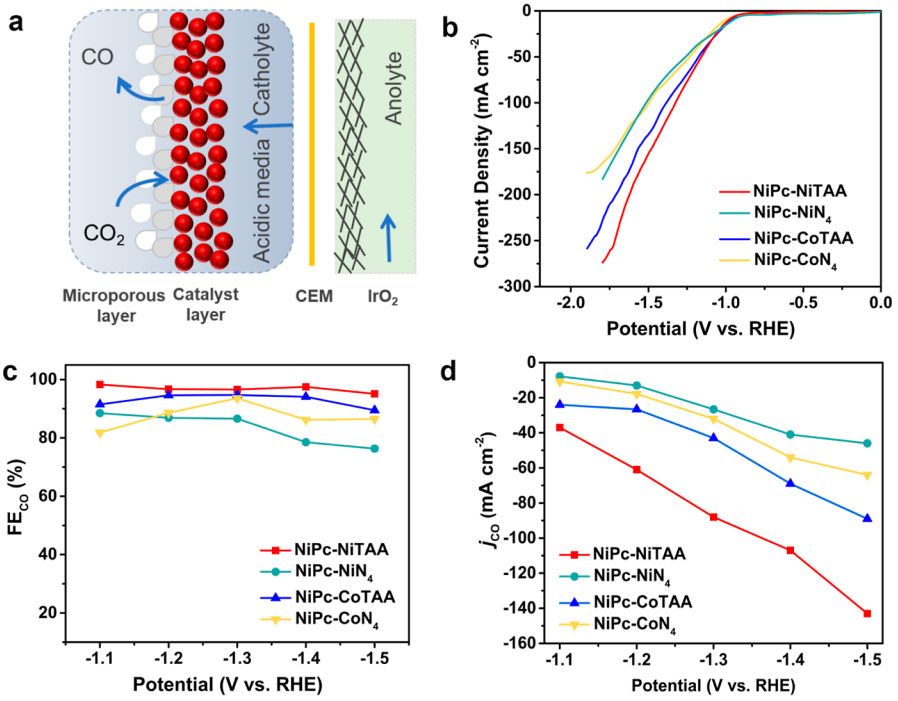

Figure 4. Electrocatalytic CO_2RR performance under acidic media (pH = 2) in the flow-cell: (a) schematic for flow-cell configuration. (b) LSV curves of NiPc−NiTAA, NiPc−NiN_4, NiPc−CoTAA, and NiPc−CoN_4 in sulfuric acid electrolyte (0.5 M K_2SO_4 with H_2SO_4 additives, pH = 2). (c) FE_{CO} for NiPc−NiTAA, NiPc−NiN_4, NiPc−CoTAA, and NiPc−CoN_4, and (d) j_{CO} for NiPc−NiTAA, NiPc−NiN_4, NiPc−CoTAA, and NiPc−CoN_4.

N═C and Ni−N dominated at 398.8 and 400.0 eV, respectively (Figure S10c).[62,63] These results indicated that Ni tetraaza[14]annulene was introduced into the framework successfully.

To explore the effect of tetraaza[14]annulene on CO_2RR performances in MCOFs, the CO_2RR activities of NiPc−NiTAA and the corresponding MOF NiPc−NiN_4 were first investigated in an acidic electrolyte including 0.5 M K_2SO_4 solution at pH = 2. A gas diffusion electrode was utilized to investigate the performance (Figure 4a and Figure S11). The potentials mentioned in this work were corrected by a reversible hydrogen electrode (RHE). The gaseous products and liquid products were confirmed by gas chromatography (GC) and ^{1}H nuclear magnetic resonance (^{1}H NMR), respectively. The GC and ^{1}H NMR results revealed that no liquid product was produced except CO and H_2 (Figure S12). The CO origination was from the CO_2 reduction rather than decomposition of the catalyst, which was proved by ^{13}C-labeling CO_2 isotope experiments (Figure S13). From linear sweep voltammetry (LSV) results in Figure 4b, NiPc−NiTAA and NiPc−CoTAA exhibited current densities higher than those of the corresponding NiPc−NiN_4 and NiPc−CoN_4 at an applied potential from −1.1 to −1.8 V, implying superior CO_2RR performance for MCOFs. Among them, NiPc−NiTAA has the largest total current density of 273.8 mA cm^{-2} at −1.8 V. Meanwhile, excellent FE_{CO} over 95% was achieved for NiPc−NiTAA in the potentials window from −1.1 V to −1.5 V, reaching the maximum FE_{CO} of 98.3% at −1.1 V (Figure 4c). Interestingly, thanks to the strong conjugation in NiPc−NiTAA, the industrial-level j_{CO} of 143.0 mA cm^{-2} was obtained, which was about 3.1 and 2.2 times larger than for NiPc−NiN_4 and NiPc−CoN_4, respectively (Figure 4d). To further determine that the activity of the CO_2RR is originated from the NiPc unit or NiTAA node or NiN_4 node, NiTAA was prepared by tetramethoxypropane (TMP) and *o*-phenylendiamine dihydrochloride (Figure S14).[60] In addition, the 2D MOF $Ni_3(HITP)_2$, containing the NiN_4 nodes, was also synthesized by 2,3,6,7,10,11-hexaaminotriphentlene hexahydrochloride and $NiCl_2{\cdot}6H_2O$ (Figure S15).[64] The CO_2RR experiments were conducted under the same conditions. As shown in Figure S16a, NiPc achieved the maximum FE_{CO} of 97.2% at −1.4 V and a j_{CO} of 63.5 mA cm^{-2} at −1.5 V. Moreover, NiTAA obtained a FE_{CO} of 86.1% at −1.3 V and a j_{CO} of −14.0 mA cm^{-2} at −1.5 V. The $Ni_3(HITP)_2$ had no activity for CO_2RR and yielded H_2 nearly 100% (Figure S17). The above results indicated that the NiPc units and NiTAA nodes collaborated to polish up the CO_2RR performance in acidic electrolyte for NiPc−NiTAA. As shown in Table S4, the excellent NiPc−NiTAA surpassed most of the catalysts in acidic reaction systems. In addition, electrocatalytic stability for MCOFs and MOFs was tested under a constant potential electrolysis at −1.1 V. As shown in Figure S18, NiPc−NiTAA showed no significant decay in FE_{CO}, which was around 92% after 6 h electrolysis, while NiPc−NiN_4 showed an obvious decline in current density and selectivity after only 2 h electrolysis. The excellent performances in selectivity, current density, and stability could reasonably be attributed to the extended in-plane d−π and macrocyclic π-conjugation in the robust NiPc−NiTAA. Furthermore, XPS, TEM, Ni K-edge EXANE and EXAFS, and PXRD for NiPc−NiTAA after the CO_2RR measurement showed no obvious changes (Figures S19−S21). The ICP value of Ni in the electrolyte after CO_2RR catalysis (Table S5) demonstrated that there was no leaching of Ni(II) ions from NiPc−NiTAA during electrocatalysis. All these results demonstrated that the introduction of nickel tetraaza[14]annulene into NiPc−MTAA could enhance the framework structure stability and thus promote the CO_2RR in an acidic electrolyte.

https://doi.org/10.1021/jacsau.4c00246
JACS Au 2024, 4, 2514−2522

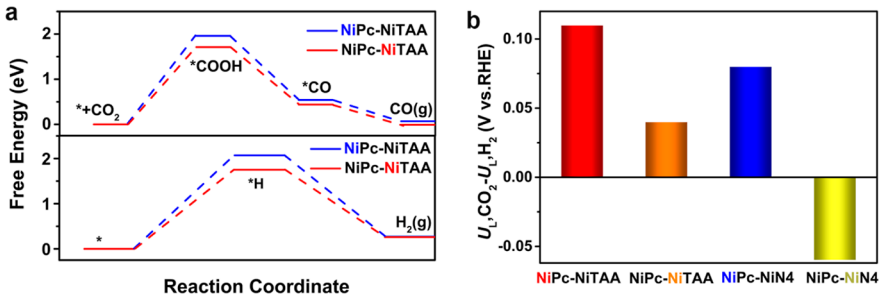

Figure 5. (a) Free energy of the CO_2RR and HER over Ni sites in NiPc−NiTAA. (b) Limiting potential difference on the Ni sites in NiPc−NiTAA and NiPc−NiN_4.

The feasibility of the CO_2RR for NiPc−NiTAA in acidic electrolyte with different pHs (1, 2, 4, and 6) and different cations (Li^+, Na^+, K^+, and Cs^+) were also investigated. As shown in Figure S22, as the pH increases from 1 to 2 to 4 and 6 at −1.1 V, the CO_2RR performance (FE_{CO} and j_{CO}) increased. Obviously, an excellent FE_{CO} up to 95% was achieved at the low pH of 2 from −1.1 to −1.5 V. The good CO_2RR performance in acidic electrolyte may be attributed to the formation of a chemically inert hydrated alkali metal ions layer at the outer Helmholtz plane, inhibiting HER and enhancing CO_2 adsorption.[24,25] However, the proton source was H^+ rather than H_3O^+ under a lower pH (pH = 1), which facilitates HER. These results indicated that the CO_2RR performance would be significantly influenced by the local pH environment (H^+ concentration). Moreover, apart from the pH, the influence of alkali metal cations was then performed. As shown in Figures S23 and S24, CO_2 electrolysis was conducted in an acidic catholyte with different 0.5 M M_2SO_4 and H_2SO_4 (M^+ = Li, Na, K, and Cs) at pH = 2. The changing trend for FE_{CO} and j_{CO} with the variation of different alkali metal ions is shown in Figure S24. As the metal ions change from Li^+ to Na^+, K^+, and Cs^+, FE_{CO} and j_{CO} increase first and a maximum value was achieved in the K^+-containing electrolyte at −1.5 V. The superior performance with K_2SO_4 solution and the poor activity in Li_2SO_4 electrolyte indicated that K^+ could enhance the CO_2RR performance in a strong acidic electrolyte with pH = 2. The result may be ascribed to a high concentration of a weak hydration shell of K^+ near the electrode surface, which endowed the hydrated K^+ with a high capability to coordinate with $*CO_2^-$ and thus more CO_2 and hydrated K^+ accumulated around the catalyst surface, thus promoting CO production.[5,28] These findings highlight that the choice of cation and pH that favored the electrolysis of CO_2 in acidic electrolyte is crucial.

For understanding the intrinsic catalytic features of MCOFs and MOFs, the electrochemical surface area and Tafel slope measurements were conducted. As shown in Figure S25, cyclic voltammetry was performed to obtain the double-layer capacitance (C_{dl}). NiPc−NiTAA presented a larger C_{dl} (8.3 mF cm^{-2}) than NiPc−NiN_4 (7.2 mF cm^{-2}). It indicated that NiPc−NiTAA had more active sites than NiPc−NiN_4 and thus larger increase in the current density for NiPc−NiTAA. Moreover, faster kinetics occurred in NiPc−NiTAA, which was proved by the Tafel slope. The Tafel slope values of NiPc−MTAA and NiPc−MN_4 were larger than 118 mV dec^{-1} (Figure S26), manifesting that *COOH generation through a proton-coupled electron transfer process (PCET) was the rate-determining steps (RDS). Both NiPc−NiTAA (125.4 mV dec^{-1}) and NiPc−CoTAA (177.6 mV dec^{-1}) presented much lower Tafel slopes in comparison with NiPc−NiN_4 (172.8 mV dec^{-1}) and NiPc−CoN_4 (182.1 mV dec^{-1}), manifesting faster kinetics for MCOFs in CO_2 conversion. This superiority might be ascribed to more electron transfer and higher conductivity of the fully π-conjugation structure of MCOFs with M-tetraaza[14]annulenes.

To detect possible reaction intermediates and investigate the mechanism during CO_2RR over NiPc−NiTAA, in situ FT-IR for NiPc−NiTAA was performed in a homemade cell (Figure S27). Figure S28 shows the strong peak centered at 1396 cm^{-1} indexed to *COOH.[35,54] Additionally, a small peak at 1982 cm^{-1} is shown, which belonged to the *CO intermediate.[65]

To further investigate the catalytic mechanism of NiPc−MTAA and NiPc−MN_4, DFT calculations were done for the free energy of the CO_2RR and HER. The RDS in the CO_2RR and HRE over MCOFs and MOFs is the formation of *COOH and *H, respectively. In Figure 5a, the*COOH formation free energies over NiPc sites and NiTAA sites in NiPc−NiTAA were 1.96 and 1.71 eV, respectively, which were lower than the corresponding free energy of formation of *H (2.07 eV for NiPc site, 1.75 eV for NiTAA site). This result indicated that NiPc−NiTAA was beneficial for the CO_2RR rather than the HER. Meanwhile, $U_L(CO_2)-U_L(H_2)$ represents the limiting potential difference of CO_2RR and HER, which was further used as an indicator and a more positive $U_L(CO_2)-U_L(H_2)$ indicated better selectivity to CO.[6] As shown in Figure 5b, the NiPc site in NiPc−NiTAA presented the most positive value (0.11 eV) among all calculated sites, further supporting the higher CO selectivity of NiPc−NiTAA. The electronic structure calculation was also performed to demonstrate the electronic structure of the metal atoms and the adsorbate. According to the projected density of states for Ni 3d orbitals and the CO_2 2p orbitals, the electronic energies became closer to the Fermi level,[7] indicating that the Ni center in the NiPc site of NiPc−NiTAA had the capability to activate CO_2, thus favoring the reactivity of Ni sites (Figure S29). Apparently, the excellent performance of NiPc−NiTAA in acidic electrolyte was mainly due to the collaboration of NiPc and NiTAA sites to reduce the energy barrier of formation of *COOH and then promote the activity.

CONCLUSIONS

In conclusion, conductive 2D NiPc-based MCOFs (NiPc−MTAA) frameworks connected with the metal tetraaza[14]-annulene linkage were constructed and employed as a highly efficient electrocatalyst for CO_2 reduction under acidic electrolyte. Compared with 2D NiPc−based MOFs (NiPc−MN_4), MCOFs exhibit good electrical conductivity and stability thanks to full in-plane π-delocalization. Thus, the

https://doi.org/10.1021/jacsau.4c00246
JACS Au 2024, 4, 2514−2522

optimal NiPc−NiTAA exhibits high selectivity toward the CO product with an excellent FE_{CO} of 95.1% and a large j_{CO} of 143.0 mA cm^{-2} at −1.5 V vs RHE and maintains its CO_2RR activity for 6 h in an acidic electrolyte, which is 3.1 times higher than for the corresponding MOF NiPc−NiN_4. The comparison tests and DFT analysis revealed that metal tetraaza[14]annulene linkage extends in-plane d−π and macrocyclic π-conjugation in NiPc−NiTAA, which facilitates the electron transfer along the bonds and thus enhances the CO_2RR performance. The NiTAA node optimizes the electron distribution of 3d orbitals, making the d-band center close to the Fermi level, and then activating CO_2 easily. This work offers a feasible way to design excellent electrocatalytic behavior of extended in-plane d−π conjugation 2D MCOFs and gives a direction to enhance the activity of electrocatalysts under acidic electrolytes.

METHODS

Synthesis of NiPc−NiTAA

Nickel octaminophthalocyanine (1 equiv), tetramethoxypropane (4 equiv), and Ni(II) acetate tetrahydrate (2 equiv) were put together into a glass tube with dimethylformamide/triethylamine (DMF/Et3N) solution. Then the tube was sonicated for 2 min. The mixture was heated to 120 °C for 5 days. The precipitated solid was collected by centrifugation. The obtained powder was dried for 12 h.

Synthesis of NiPc−NiN_4

NiCl2·6H2O and $NH_3{\cdot}H_2O$ were added together with NiPc−$(NH2)_8$ into degassed DMSO. The mixture was reacted at 60 °C for 12 h. After the reaction, the solid was collected as a black powder.

Synthesis of NiPc−CoTAA

A mixture of nickel octaminophthalocyanine (1 equiv), tetramethoxypropane (4 equiv), and Co(II) acetate tetrahydrate (2 equiv) was put together into a glass tube with DMF/Et3N solution. Then the tube was sonicated for 2 min. The mixture was heated at 120 °C for 5 days. The precipitated solid was collected by centrifugation. The obtained powder was dried for 12 h.

Synthesis of NiPc−CoN_4

NiPc−$(NH2)_8$ and Co(II) acetate tetrahydrate (2.5 equiv) were added into DMSO. The mixture was sonicated and then reacted at 65 °C for 48 h with the flask loosely capped. Finally, the dark green to black precipitate was filtered.

ASSOCIATED CONTENT

Supporting Information

The Supporting Information is available free of charge at https://pubs.acs.org/doi/10.1021/jacsau.4c00246.

Details for electrochemical measurements, preparation, and characterizations of materials (PDF)

AUTHOR INFORMATION

Corresponding Author

Rong Cao − *State Key Laboratory of Structural Chemistry, Fujian Institute of Research on the Structure of Matter, Chinese Academy of Sciences, Fujian, Fuzhou 350002, P. R. China; Fujian Science & Technology Innovation Laboratory for Optoelectronic Information of China Fuzhou, Fujian 350108, P. R. China; University of Chinese Academy of Sciences, Beijing 100049, P. R. China;* orcid.org/0000-0002-2398-399X; Email: rcao@fjirsm.ac.cn

Authors

Chang-Pu Wan − *State Key Laboratory of Structural Chemistry, Fujian Institute of Research on the Structure of Matter, Chinese Academy of Sciences, Fujian, Fuzhou 350002, P. R. China; University of Chinese Academy of Sciences, Beijing 100049, P. R. China*

Hui Guo − *State Key Laboratory of Structural Chemistry, Fujian Institute of Research on the Structure of Matter, Chinese Academy of Sciences, Fujian, Fuzhou 350002, P. R. China; University of Chinese Academy of Sciences, Beijing 100049, P. R. China*

Duan-Hui Si − *State Key Laboratory of Structural Chemistry, Fujian Institute of Research on the Structure of Matter, Chinese Academy of Sciences, Fujian, Fuzhou 350002, P. R. China*

Shui-Ying Gao − *State Key Laboratory of Structural Chemistry, Fujian Institute of Research on the Structure of Matter, Chinese Academy of Sciences, Fujian, Fuzhou 350002, P. R. China;* orcid.org/0000-0002-1711-1319

Yuan-Biao Huang − *State Key Laboratory of Structural Chemistry, Fujian Institute of Research on the Structure of Matter, Chinese Academy of Sciences, Fujian, Fuzhou 350002, P. R. China; Fujian Science & Technology Innovation Laboratory for Optoelectronic Information of China Fuzhou, Fujian 350108, P. R. China; University of Chinese Academy of Sciences, Beijing 100049, P. R. China;* orcid.org/0000-0003-4680-2976

Complete contact information is available at: https://pubs.acs.org/10.1021/jacsau.4c00246

Author Contributions

C.-P.W. and H.G. contributed equally. All authors have given approval to the final version of the manuscript. CRediT: **Chang-Pu Wan** data curation, writing-original draft; **Hui Guo** writing-original draft; **Duan-Hui Si** data curation; **Shui-Ying Gao** funding acquisition; **Rong Cao** funding acquisition, supervision; **Yuan-Biao Huang** conceptualization, writing-review & editing.

Notes

The authors declare no competing financial interest.

ACKNOWLEDGMENTS

We acknowledge the financial support from the National Key Research and Development Program of China (2021YFA1501500, 2023YFA1507904), NSFC (U22A20436, 22071245, 22033008, 22220102005), and Fujian Science & Technology Innovation Laboratory for Optoelectronic Information of China (2021ZZ103). We thank the beamline BL14W1 station for XAFS measurements at the Shanghai Synchrotron Radiation Facility, China.

REFERENCES

(1) Birdja, Y. Y.; Pérez-Gallent, E.; Figueiredo, M. C.; Göttle, A. J.; Calle-Vallejo, F.; Koper, M. T. M. Advances and Challenges in Understanding the Electrocatalytic Conversion of Carbon Dioxide to Fuels. *Nat. Energy* **2019**, *4* (9), 732−745.

(2) Wu, Q. J.; Liang, J.; Huang, Y. B.; Cao, R. Thermo-Electro-and Photocatalytic CO_2 Conversion to Value-Added Products over Porous Metal/Covalent Organic Frameworks. *Acc. Chem. Res.* **2022**, *55* (20), 2978−2997.

(3) Li, S.; Dong, X.; Zhao, Y.; Mao, J.; Chen, W.; Chen, A.; Song, Y.; Li, G.; Jiang, Z.; Wei, W.; Sun, Y. Chloride Ion Adsorption Enables

Ampere-Level CO_2 Electroreduction over Silver Hollow Fiber. *Angew. Chem., Int. Ed.* **2022**, *61* (42), No. e202210432.
(4) Li, S.; Chen, W.; Dong, X.; Zhu, C.; Chen, A.; Song, Y.; Li, G.; Wei, W.; Sun, Y. Hierarchical Micro/Nanostructured Silver Hollow Fiber Boosts Electroreduction of Carbon Dioxide. *Nat. Commun.* **2022**, *13* (1), 3080.
(5) Ni, W.; Guan, Y.; Chen, H.; Zhang, Y.; Wang, S.; Zhang, S. Molecular Engineering of Cation Solvation Structure for Highly Selective Carbon Dioxide Electroreduction. *Angew. Chem., Int. Ed.* **2023**, *62* (37), No. e202303233.
(6) Wu, Q. J.; Si, D. H.; Wu, Q.; Dong, Y. L.; Cao, R.; Huang, Y. B. Boosting Electroreduction of CO_2 over Cationic Covalent Organic Frameworks: Hydrogen Bonding Effects of Halogen Ions. *Angew. Chem., Int. Ed.* **2023**, *62* (7), No. e202215687.
(7) Li, N.; Si, D.-H.; Wu, Q. j.; Wu, Q.; Huang, Y. B.; Cao, R. Boosting Electrocatalytic CO_2 Reduction with Conjugated Bimetallic Co/Zn Polyphthalocyanine Frameworks. *CCS Chem.* **2023**, *5* (5), 1130−1143.
(8) Haaring, R.; Kang, P. W.; Guo, Z.; Lee, J. W.; Lee, H. Developing Catalysts Integrated in Gas-Diffusion Electrodes for CO_2 Electrolyzers. *Acc. Chem. Res.* **2023**, *56* (19), 2595−2605.
(9) Wang, Q.; Dai, M.; Li, H.; Lu, Y. R.; Chan, T. S.; Ma, C.; Liu, K.; Fu, J.; Liao, W.; Chen, S.; Pensa, E.; Wang, Y.; Zhang, S.; Sun, Y.; Cortés, E.; Liu, M. Asymmetric Coordination Induces Electron Localization at Ca Sites for Robust CO_2 Electroreduction to CO. *Adv. Mater.* **2023**, *35* (21), 2300695.
(10) Wang, Q.; Liu, K.; Hu, K.; Cai, C.; Li, H.; Li, H.; Herran, M.; Lu, Y.-R.; Chan, T.-S.; Ma, C.; Fu, J.; Zhang, S.; Liang, Y.; Cortés, E.; Liu, M. Attenuating Metal-Substrate Conjugation in Atomically Dispersed Nickel Catalysts for Electroreduction of CO_2 to CO. *Nat. Commun.* **2022**, *13* (1), 6082.
(11) Jones, C. W. Recent Developments in CO_2 Capture and Conversion. *JACS Au.* **2023**, *3* (6), 1536−1538.
(12) Yu, S.; Louisia, S.; Yang, P. The Interactive Dynamics of Nanocatalyst Structure and Microenvironment During Electrochemical CO_2 Conversion. *JACS Au.* **2022**, *2* (3), 562−572.
(13) Endrődi, B.; Samu, A.; Kecsenovity, E.; Halmágyi, T.; Sebők, D.; Janáky, C. Operando Cathode Activation with Alkali Metal Cations for High Current Density Operation of Water-Fed Zero-Gap Carbon Dioxide Electrolysers. *Nat. Energy* **2021**, *6* (4), 439−448.
(14) Wei, P.; Gao, D.; Liu, T.; Li, H.; Sang, J.; Wang, C.; Cai, R.; Wang, G.; Bao, X. Coverage-Driven Selectivity Switch from Ethylene to Acetate in High-Rate CO_2/CO Electrolysis. *Nat. Nanotechnol.* **2023**, *18* (3), 299−306.
(15) Li, W.; Yin, Z.; Gao, Z.; Wang, G.; Li, Z.; Wei, F.; Wei, X.; Peng, H.; Hu, X.; Xiao, L.; Lu, J.; Zhuang, L. Bifunctional Ionomers for Efficient Co-Electrolysis of CO_2 and Pure Water Towards Ethylene Production at Industrial-Scale Current Densities. *Nat. Energy* **2022**, *7* (9), 835−843.
(16) Ozden, A.; García de Arquer, F. P.; Huang, J. E.; Wicks, J.; Sisler, J.; Miao, R. K.; O'Brien, C. P.; Lee, G.; Wang, X.; Ip, A. H.; Sargent, E. H.; Sinton, D. Carbon-Efficient Carbon Dioxide Electrolysers. *Nat. Sustain.* **2022**, *5* (7), 563−573.
(17) Wen, M.; Sun, N.; Jiao, L.; Zang, S. Q.; Jiang, H. L. Microwave-Assisted Rapid Synthesis of Mof-Based Single-Atom Ni Catalyst for CO_2 Electroreduction at Ampere-Level Current. *Angew. Chem., Int. Ed.* **2024**, *63* (10), No. e202318338.
(18) Shah, S. S. A.; Najam, T.; Wen, M.; Zang, S. Q.; Waseem, A.; Jiang, H. L. Metal-Organic Framework-Based Electrocatalysts for CO_2 Reduction. *Small Structures.* **2021**, *3* (5), 2100090.
(19) Perazio, A.; Creissen, C. E.; Rivera de la Cruz, J. G.; Schreiber, M. W.; Fontecave, M. Acidic Electroreduction of CO_2 to Multi-Carbon Products with CO_2 Recovery and Recycling from Carbonate. *ACS Energy Lett.* **2023**, *8* (7), 2979−2985.
(20) Huang, J. E.; Li, F.; Ozden, A.; Sedighian Rasouli, A.; García de Arquer, F. P.; Liu, S.; Zhang, S.; Luo, M.; Wang, X.; Lum, Y.; Xu, Y.; Bertens, K.; Miao, R. K.; Dinh, C. T.; Sinton, D.; Sargent, E. H. CO_2 Electrolysis to Multicarbon Products in Strong Acid. *Science* **2021**, *372* (6546), 1074−1078.
(21) Fan, M.; Huang, J. E.; Miao, R. K.; Mao, Y.; Ou, P.; Li, F.; Li, X. Y.; Cao, Y.; Zhang, Z.; Zhang, J.; Yan, Y.; Ozden, A.; Ni, W.; Wang, Y.; Zhao, Y.; Chen, Z.; Khatir, B.; O'Brien, C. P.; Xu, Y.; Xiao, Y. C.; Waterhouse, G. I. N.; Golovin, K.; Wang, Z.; Sargent, E. H.; Sinton, D. Cationic-Group-Functionalized Electrocatalysts Enable Stable Acidic CO_2 Electrolysis. *Nat. Catal.* **2023**, *6* (9), 763−772.
(22) Jiang, Z.; Zhang, Z.; Li, H.; Tang, Y.; Yuan, Y.; Zao, J.; Zheng, H.; Liang, Y. Molecular Catalyst with near 100% Selectivity for CO_2 Reduction in Acidic Electrolytes. *Adv. Energy Mater.* **2022**, *13* (6), 2203603.
(23) Lee, S. Y.; Kim, J.; Bak, G.; Lee, E.; Kim, D.; Yoo, S.; Kim, J.; Yun, H.; Hwang, Y. J. Probing Cation Effects on *CO Intermediates from Electroreduction of CO_2 through Operando Raman Spectroscopy. *J. Am. Chem. Soc.* **2023**, *145* (42), 23068−23075.
(24) Li, H.; Li, H.; Wei, P.; Wang, Y.; Zang, Y.; Gao, D.; Wang, G.; Bao, X. Tailoring Acidic Microenvironments for Carbon-Efficient CO_2 Electrolysis over a Ni-N-C Catalyst in a Membrane Electrode Assembly Electrolyzer. *Energy Environ. Sci.* **2023**, *16* (4), 1502−1510.
(25) Li, Z.; Sun, B.; Xiao, D.; Wang, Z.; Liu, Y.; Zheng, Z.; Wang, P.; Dai, Y.; Cheng, H.; Huang, B. Electron-Rich Bi Nanosheets Promote $Co2^{\cdot-}$ Formation for High-Performance and pH-Universal Electrocatalytic CO_2 Reduction. *Angew. Chem., Int. Ed.* **2023**, *62* (11), No. e202217569.
(26) Liu, Z.; Yan, T.; Shi, H.; Pan, H.; Cheng, Y.; Kang, P. Acidic Electrocatalytic CO_2 Reduction Using Space-Confined Nanoreactors. *ACS Appl. Mater. Inter.* **2022**, *14* (6), 7900−7908.
(27) Ma, Z.; Yang, Z.; Lai, W.; Wang, Q.; Qiao, Y.; Tao, H.; Lian, C.; Liu, M.; Ma, C.; Pan, A.; Huang, H. CO_2 Electroreduction to Multicarbon Products in Strongly Acidic Electrolyte Via Synergistically Modulating the Local Microenvironment. *Nat. Commun.* **2022**, *13* (1), 7596.
(28) Monteiro, M. C. O.; Dattila, F.; López, N.; Koper, M. T. M. The Role of Cation Acidity on the Competition between Hydrogen Evolution and CO_2 Reduction on Gold Electrodes. *J. Am. Chem. Soc.* **2022**, *144* (4), 1589−1602.
(29) Pan, B.; Fan, J.; Zhang, J.; Luo, Y.; Shen, C.; Wang, C.; Wang, Y.; Li, Y. Close to 90% Single-Pass Conversion Efficiency for CO_2 Electroreduction in an Acid-Fed Membrane Electrode Assembly. *ACS Energy Lett.* **2022**, *7* (12), 4224−4231.
(30) Sheng, X.; Ge, W.; Jiang, H.; Li, C. Engineering the Ni-N-C Catalyst Microenvironment Enabling CO_2 Electroreduction with Nearly 100% CO Selectivity in Acid. *Adv. Mater.* **2022**, *34* (38), 2201295.
(31) Wang, Z.; Hou, P.; Wang, Y.; Xiang, X.; Kang, P. Acidic Electrochemical Reduction of CO_2 Using Nickel Nitride on Multiwalled Carbon Nanotube as Selective Catalyst. *ACS Sustain. Chem. Eng.* **2019**, *7* (6), 6106−6112.
(32) Xue, H.; Zhao, Z. H.; Liao, P. Q.; Chen, X. M. Ship-in-a-Bottle" Integration of Ditin(IV) Sites into a Metal-Organic Framework for Boosting Electroreduction of CO_2 in Acidic Electrolyte. *J. Am. Chem. Soc.* **2023**, *145* (31), 16978−16982.
(33) Monteiro, M. C. O.; Philips, M. F.; Schouten, K. J. P.; Koper, M. T. M. Efficiency and Selectivity of CO_2 Reduction to CO on Gold Gas Diffusion Electrodes in Acidic Media. *Nat. Commun.* **2021**, *12* (1), 4943.
(34) Xie, Y.; Ou, P.; Wang, X.; Xu, Z.; Li, Y. C.; Wang, Z.; Huang, J. E.; Wicks, J.; McCallum, C.; Wang, N.; Wang, Y.; Chen, T.; Lo, B. T. W.; Sinton, D.; Yu, J. C.; Wang, Y.; Sargent, E. H. High Carbon Utilization in CO_2 Reduction to Multi-Carbon Products in Acidic Media. *Nat. Catal.* **2022**, *5* (6), 564−570.
(35) Wu, Q.; Si, D. H.; Liang, J.; Huang, Y. B.; Cao, R. Highly Efficient Electrocatalytic CO_2 Reduction over Pyrolysis-Free Conjugated Metallophthalocyanine Networks in Full pH Range. *Appl. Catal. B: Environ.* **2023**, *333*, 122803.
(36) Wu, Q.; Liang, J.; Han, L. L.; Huang, Y. B.; Cao, R. A Highly Efficient Atomic Nickel Catalyst for CO_2 Electroreduction in Acidic Electrolyte. *Chem. Commun.* **2023**, *59* (34), 5102−5105.
(37) Qiao, Y.; Lai, W.; Huang, K.; Yu, T.; Wang, Q.; Gao, L.; Yang, Z.; Ma, Z.; Sun, T.; Liu, M.; Lian, C.; Huang, H. Engineering the

https://doi.org/10.1021/jacsau.4c00246
JACS Au 2024, 4, 2514−2522

Local Microenvironment over Bi Nanosheets for Highly Selective Electrocatalytic Conversion of CO_2 to HCOOH in Strong Acid. *ACS Catal.* **2022**, *12* (4), 2357−2364.
(38) Wu, Y.; Kamiya, K.; Hashimoto, T.; Sugimoto, R.; Harada, T.; Fujii, K.; Nakanishi, S. Electrochemical CO_2 Reduction Using Gas Diffusion Electrode Loading Ni-Doped Covalent Triazine Frameworks in Acidic Electrolytes. *Electrochemistry.* **2020**, *88* (5), 359−364.
(39) Bondue, C. J.; Graf, M.; Goyal, A.; Koper, M. T. M. Suppression of Hydrogen Evolution in Acidic Electrolytes by Electrochemical CO_2 Reduction. *J. Am. Chem. Soc.* **2021**, *143* (1), 279−285.
(40) Gu, J.; Liu, S.; Ni, W.; Ren, W.; Haussener, S.; Hu, X. Modulating Electric Field Distribution by Alkali Cations for CO_2 Electroreduction in Strongly Acidic Medium. *Nat. Catal.* **2022**, *5* (4), 268−276.
(41) Liang, Z.; Wang, H. Y.; Zheng, H.; Zhang, W.; Cao, R. Porphyrin-Based Frameworks for Oxygen Electrocatalysis and Catalytic Reduction of Carbon Dioxide. *Chem. Soc. Rev.* **2021**, *50* (4), 2540−2581.
(42) Han, B.; Jin, Y.; Chen, B.; Zhou, W.; Yu, B.; Wei, C.; Wang, H.; Wang, K.; Chen, Y.; Chen, B.; Jiang, J. Maximizing Electroactive Sites in a Three-Dimensional Covalent Organic Framework for Significantly Improved Carbon Dioxide Reduction Electrocatalysis. *Angew. Chem., Int. Ed.* **2021**, *61* (1), No. e202114244.
(43) Ren, Z.; Zhao, B.; Xie, J. Designing N-Confused Metalloporphyrin-Based Covalent Organic Frameworks for Enhanced Electrocatalytic Carbon Dioxide Reduction. *Small* **2023**, *19* (33), 2301818.
(44) Zhang, M. D.; Huang, J. R.; Shi, W.; Liao, P. Q.; Chen, X. M. Self-Accelerating Effect in a Covalent-Organic Framework with Imidazole Groups Boosts Electroreduction of CO_2 to CO. *Angew. Chem., Int. Ed.* **2023**, *62* (42), No. e202308195.
(45) Han, B.; Ding, X.; Yu, B.; Wu, H.; Zhou, W.; Liu, W.; Wei, C.; Chen, B.; Qi, D.; Wang, H.; Wang, K.; Chen, Y.; Chen, B.; Jiang, J. Two-Dimensional Covalent Organic Frameworks with Cobalt(II)-Phthalocyanine Sites for Efficient Electrocatalytic Carbon Dioxide Reduction. *J. Am. Chem. Soc.* **2021**, *143* (18), 7104−7113.
(46) Zhang, M. D.; Huang, J. R.; Shi, W.; Liao, P. Q.; Chen, X. M. Synergistic Effect in a Metal-Organic Framework Boosting the Electrochemical CO_2 Overall Splitting. *J. Am. Chem. Soc.* **2023**, *145* (4), 2439−2447.
(47) Chen, Z.; Wang, K.; Tang, Y.; Li, L.; Hu, X.; Han, M.; Guo, Z.; Zhan, H.; Chen, B. Reticular Synthesis of One-Dimensional Covalent Organic Frameworks with 4-C Sql Topology for Enhanced Fluorescence Emission. *Angew. Chem., Int. Ed.* **2022**, *62* (1), No. e202213268.
(48) Huang, C.; Sun, W.; Jin, Y.; Guo, Q.; Mücke, D.; Chu, X.; Liao, Z.; Chandrasekhar, N.; Huang, X.; Lu, Y.; Chen, G.; Wang, M.; Liu, J.; Zhang, G.; Yu, M.; Qi, H.; Kaiser, U.; Xu, G.; Feng, X.; Dong, R. A General Synthesis of Nanostructured Conductive Metal-Organic Frameworks from Insulating MOF Precursors for Supercapacitors and Chemiresistive Sensors. *Angew. Chem., Int. Ed.* **2023**, *63*, No. e202313591.
(49) Meng, Z.; Luo, J.; Li, W.; Mirica, K. A. Hierarchical Tuning of the Performance of Electrochemical Carbon Dioxide Reduction Using Conductive Two-Dimensional Metallophthalocyanine Based Metal-Organic Frameworks. *J. Am. Chem. Soc.* **2020**, *142* (52), 21656−21669.
(50) Ding, M.; Flaig, R. W.; Jiang, H.-L.; Yaghi, O. M. Carbon Capture and Conversion Using Metal-Organic Frameworks and MOF-Based Materials. *Chem. Soc. Rev.* **2019**, *48* (10), 2783−2828.
(51) Lyu, H.; Chen, O. I. F.; Hanikel, N.; Hossain, M. I.; Flaig, R. W.; Pei, X.; Amin, A.; Doherty, M. D.; Impastato, R. K.; Glover, T. G.; Moore, D. R.; Yaghi, O. M. Carbon Dioxide Capture Chemistry of Amino Acid Functionalized Metal-Organic Frameworks in Humid Flue Gas. *J. Am. Chem. Soc.* **2022**, *144* (5), 2387−2396.
(52) Qiao, G. Y.; Guan, D.; Yuan, S.; Rao, H.; Chen, X.; Wang, J. A.; Qin, J. S.; Xu, J. J.; Yu, J. Perovskite Quantum Dots Encapsulated in a Mesoporous Metal-Organic Framework as Synergistic Photocathode Materials. *J. Am. Chem. Soc.* **2021**, *143* (35), 14253−14260.
(53) Zhang, Q.; Yu, J.; Corma, A. Applications of Zeolites to C1 Chemistry: Recent Advances, Challenges, and Opportunities. *Adv. Mater.* **2020**, *32* (44), 2002927.
(54) Wu, Q. J.; Si, D. H.; Ye, S.; Dong, Y. L.; Cao, R.; Huang, Y. B. Photocoupled Electroreduction of CO_2 over Photosensitizer-Decorated Covalent Organic Frameworks. *J. Am. Chem. Soc.* **2023**, *145* (36), 19856−19865.
(55) Tian, X.; Huang, X.; Shi, J. W.; Zhou, J.; Guo, C.; Wang, R.; Wang, Y. R.; Lu, M.; Li, Q.; Chen, Y.; Li, S. L.; Lan, Y. Q. Implanting Built-in Electric Field in Heterometallic Phthalocyanine Covalent Organic Frameworks for Light-Assisted CO_2 Electroreduction. *CCS Chem.* **2022**, *5* (11), 2557−2566.
(56) Huang, N.; Lee, K. H.; Yue, Y.; Xu, X.; Irle, S.; Jiang, Q.; Jiang, D. A Stable and Conductive Metallophthalocyanine Framework for Electrocatalytic Carbon Dioxide Reduction in Water. *Angew. Chem., Int. Ed.* **2020**, *59* (38), 16587−16593.
(57) Dong, J.; Han, X.; Liu, Y.; Li, H.; Cui, Y. Metal-Covalent Organic Frameworks (MCOFs): A Bridge between Metal-Organic Frameworks and Covalent Organic Frameworks. *Angew. Chem., Int. Ed.* **2020**, *59* (33), 13722−13733.
(58) Zhang, M. D.; Si, D. H.; Yi, J. D.; Yin, Q.; Huang, Y. B.; Cao, R. Conductive Phthalocyanine-Based Metal-Organic Framework as a Highly Efficient Electrocatalyst for Carbon Dioxide Reduction Reaction. *Sci. Chi. Chem.* **2021**, *64* (8), 1332−1339.
(59) Yue, Y.; Cai, P.; Xu, X.; Li, H.; Chen, H.; Zhou, H. C.; Huang, N. Conductive Metallophthalocyanine Framework Films with High Carrier Mobility as Efficient Chemiresistors. *Angew. Chem., Int. Ed.* **2021**, *60* (19), 10806−10813.
(60) Jiang, Y.; Oh, I.; Joo, S. H.; Buyukcakir, O.; Chen, X.; Lee, S. H.; Huang, M.; Seong, W. K.; Kwak, S. K.; Yoo, J. W.; Ruoff, R. S. Partial Oxidation-Induced Electrical Conductivity and Paramagnetism in a Ni(II) Tetraaza[14]Annulene-Linked Metal Organic Framework. *J. Am. Chem. Soc.* **2019**, *141* (42), 16884−16893.
(61) Yi, J. D.; Si, D. H.; Xie, R.; Yin, Q.; Zhang, M. D.; Wu, Q.; Chai, G. L.; Huang, Y. B.; Cao, R. Conductive Two-Dimensional Phthalocyanine-Based Metal-Organic Framework Nanosheets for Efficient Electroreduction of CO_2. *Angew. Chem., Int. Ed.* **2021**, *60* (31), 17108−17114.
(62) Wang, M.; Ballabio, M.; Wang, M.; Lin, H. H.; Biswal, B. P.; Han, X.; Paasch, S.; Brunner, E.; Liu, P.; Chen, M.; Bonn, M.; Heine, T.; Zhou, S.; Canovas, E.; Dong, R.; Feng, X. Unveiling Electronic Properties in Metal-Phthalocyanine-Based Pyrazine-Linked Conjugated Two-Dimensional Covalent Organic Frameworks. *J. Am. Chem. Soc.* **2019**, *141* (42), 16810−16816.
(63) Wang, X.; Chang, G.; Liu, C.; Li, R.; Jin, Y.; Ding, X.; Liu, X.; Wang, H.; Wang, T.; Jiang, J. Chemical Conversion of Metal-Organic Frameworks into Hemi-Covalent Organic Frameworks. *Inorg. Chem. Front.* **2022**, *9* (18), 4776−4784.
(64) Chen, T.; Dou, J. H.; Yang, L.; Sun, C.; Libretto, N. J.; Skorupskii, G.; Miller, J. T.; Dincă, M. Continuous Electrical Conductivity Variation in M_3(Hexaiminotriphenylene)$_2$ (M = Co, Ni, Cu) MOF Alloys. *J. Am. Chem. Soc.* **2020**, *142* (28), 12367−12373.
(65) Zhu, S.; Jiang, B.; Cai, W. B.; Shao, M. Direct Observation on Reaction Intermediates and the Role of Bicarbonate Anions in CO_2 Electrochemical Reduction Reaction on Cu Surfaces. *J. Am. Chem. Soc.* **2017**, *139* (44), 15664−15667.

https://doi.org/10.1021/jacsau.4c00246
JACS Au 2024, 4, 2514−2522